Title

Estimating a size-specific dose for helical head CT examinations using Monte Carlo simulation methods

Journal

Medical Physics, 46(2)

ISSN

0094-2405

Authors

Hardy, Anthony J

Bostani, Maryam

Hernandez, Andrew M

et al.

Publication Date

2019-02-01

DOI

10.1002/mp.13301

Peer reviewed

Estimating a size-specific dose for helical head CT examinations using Monte Carlo simulation methods

Anthony J. Hardy[a] and Maryam Bostani
Department of Radiology, David Geffen School of Medicine, University of California, Los Angeles, Los Angeles, CA 90024, USA
Physics and Biology in Medicine Graduate Program, David Geffen School of Medicine, University of California, Los Angeles, Los Angeles, CA 90024, USA

Andrew M. Hernandez
Departments of Radiology and Biomedical Engineering, Biomedical Engineering Graduate Group, University of California Davis, Sacramento, CA 95817, USA

Maria Zankl
Helmholtz Zentrum München, German Research Center for Environmental Health (GmbH), Institute of Radiation Protection, Ingolstaedter Landstrasse 1, Neuherberg 85764, Germany

Cynthia McCollough
Department of Radiology, Mayo Clinic, Rochester, MN 55905, USA

Chris Cagnon
Department of Radiology, David Geffen School of Medicine, University of California, Los Angeles, Los Angeles, CA 90024, USA
Physics and Biology in Medicine Graduate Program, David Geffen School of Medicine, University of California, Los Angeles, Los Angeles, CA 90024, USA

John M. Boone
Departments of Radiology and Biomedical Engineering, Biomedical Engineering Graduate Group, University of California Davis, Sacramento, CA 95817, USA

Michael McNitt-Gray
Department of Radiology, David Geffen School of Medicine, University of California, Los Angeles, Los Angeles, CA 90024, USA
Physics and Biology in Medicine Graduate Program, David Geffen School of Medicine, University of California, Los Angeles, Los Angeles, CA 90024, USA

(Received 10 May 2018; revised 22 October 2018; accepted for publication 23 October 2018; published 21 December 2018)

Purpose: Size-specific dose estimates (SSDE) conversion factors have been determined by AAPM Report 204 to adjust $CTDI_{vol}$ to account for patient size but were limited to body CT examinations. The purpose of this work was to determine conversion factors that could be used for an SSDE for helical, head CT examinations for patients of different sizes.

Methods: Validated Monte Carlo (MC) simulation methods were used to estimate dose to the center of the scan volume from a routine, helical head examination for a group of patient models representing a range of ages and sizes. Ten GSF/ICRP voxelized phantom models and five pediatric voxelized patient models created from CT image data were used in this study. CT scans were simulated using a Siemens multidetector row CT equivalent source model. Scan parameters were taken from the AAPM Routine Head protocols for a fixed tube current (FTC), helical protocol, and scan lengths were adapted to the anatomy of each patient model. MC simulations were performed using mesh tallies to produce voxelized dose distributions for the entire scan volume of each model. Three tally regions were investigated: (1) a small 0.6 cc volume at the center of the scan volume, (2) 0.8–1.0 cm axial slab at the center of the scan volume, and (3) the entire scan volume. Mean dose to brain parenchyma for all three regions was calculated. Mean bone dose and a mass-weighted average dose, consisting of brain parenchyma and bone, were also calculated for the slab in the central plane and the entire scan volume. All dose measures were then normalized by $CTDI_{vol}$ for the 16 cm phantom ($CTDI_{vol,16}$). Conversion factors were determined by calculating the relationship between normalized doses and water equivalent diameter (D_w).

Results: $CTDI_{vol,16}$-normalized mean brain parenchyma dose values within the 0.6 cc volume, 0.8–1.0 cm central axial slab, and the entire scan volume, when parameterized by D_w, had an exponential relationship with a coefficient of determination (R^2) of 0.86, 0.84, and 0.88, respectively. There was no statistically significant difference between the conversion factors resulting from these three different tally regions. Exponential relationships between $CTDI_{vol,16}$-normalized mean bone doses had R^2 values of 0.83 and 0.87 for the central slab and for the entire scan volume, respectively. $CTDI_{vol,16}$-normalized mass-weighted average doses had R^2 values of 0.39 and 0.51 for the central slab and for the entire scan volume, respectively.

Conclusions: Conversion factors that describe the exponential relationship between $CTDI_{vol,16}$-normalized mean brain dose and a size metric (D_w) for helical head CT examinations have been reported for two different interpretations of the center of the scan volume. These dose descriptors have been extended to describe the dose to bone in the center of the scan volume as well as a mass-weighted average dose to brain and bone. These may be used, when combined with other efforts, to develop an SSDE dose coefficients for routine, helical head CT examinations. © *2018 American Association of Physicists in Medicine* [https://doi.org/10.1002/mp.13301]

Key words: head CT, Monte Carlo dose simulations, size-specific dose estimate

1. INTRODUCTION

A recent study conducted by the University of California Dose Optimization and Standardization Endeavor (UC Dose) summarizing CT doses across 12 University of California medical centers found that head scans comprised 16% of all adult CT examinations.[1] The same study also found that the most frequent area imaged in pediatric patients was the head, accounting for 33% of the total procedures administered.[1] The fact that radiation exposure from head CT examinations is a large contributor to the total medical radiation exposures underscores the need for accurate patient dose assessments from head CT procedures, particularly for younger patients.

The radiation dose metric commonly reported on most scanners is the volume computed tomography dose index ($CTDI_{vol}$).[2,3] This metric, however, is a measure of dose to a reference phantom, not a measure of patient dose.[2,3] Turner et al. showed that utilizing $CTDI_{vol}$ as normalization metric for Monte Carlo (MC)-simulated organ doses from abdominal CT scans compensated both for the differences among scanner manufacturers and reduced the variation in organ doses across scanners from 31.5% down to 5.2%.[4] Subsequently, AAPM Report 204 developed the size-specific dose estimate (SSDE) quantity to adjust $CTDI_{vol}$ using a set of $CTDI_{vol}$-to-patient-dose conversion coefficients from either the 32 cm CTDI reference phantom ($CTDI_{vol,32}$) or the 16 cm phantom ($CTDI_{vol,16}$) to account for patient size in adult and pediatric body CT examinations, respectively.[5] SSDE "...provides an estimate of the dose at the center of the scanned region (along z) in the patient" and is defined as the patient dose estimate that takes into account corrections based on patient size by AAPM Report 204.[5] Although SSDE has been shown to be a good substitute for organ dose in the context of abdominal scans,[6] the work of AAPM Report 204 was limited only to body CT examinations.

The work of McMillan et al. in 2014 sought to extend the approach developed by Turner et al. and used in AAPM Report 204 for the body to investigate organs of interest in the head, including the brain and the lens of eye, for routine helical and axial acquisitions.[7] In that study, strong predictive exponential correlations were observed when MC-simulated organ doses from detailed voxelized phantoms were normalized by $CTDI_{vol,16}$ and were parameterized by water equivalent diameter (D_w) as a metric of patient size,[8] yielding coefficients of determination (R^2) of 0.93 for whole brain dose for helical scans.[7] While predictive correlations were determined by McMillan et al.[5], that work focused on organ doses rather than dose to the center of the scan volume, the latter being consistent with SSDE as defined in AAPM Report 204.

Therefore, the purpose of this current study was to estimate dose to the "center of the scan volume" for helical head CT examinations that can be used to help determine conversion factors for an SSDE of the head. AAPM Report 204 states that the size-specific dose estimate (SSDE) gives an estimate of the dose at "the center of the scanned region (along z) in the patient."[5] However, for helical head CT examinations, the definition of the "center of the scanned region (along z)" is open to several interpretations, which are explored in this investigation to determine if there is difference in results based on these interpretations. As such, this work employed voxelized patient models along with MC simulation techniques with mesh tallies of the entire head to produce voxelized dose distributions wherein two different interpretations of "center of the scan volume" were investigated: (1) a small central region within the brain parenchyma and (2) a central slab comprising both brain parenchyma and bone of the cranium. Additionally, the entire scan volume was also investigated for sake of comparison and completeness. In the case of the central slab, as well for the entire scan volume, doses both to the brain parenchyma and bone were also estimated separately. To account for the dose deposited in both the brain parenchyma and bone in the head, a mass-weighted average dose comprising both brain parenchyma and bone was devised to account for the presence of both brain parenchyma and bone within the slab tally region as well as for the entire scan volume. In a manner similar to that used in AAPM Report 204, all doses were normalized by $CTDI_{vol,16}$ and were parameterized in an exponential fashion with D_w.

2. MATERIALS AND METHODS

2.A. Patient models

Ten voxelized phantom models from the GSF (Gesellschaft für Strahlen-und Umweltforschung; National Research Centre for Environment and Health — current name: Helmholtz Zentrum München, German Research Center for Environment Health, Institute of Radiation Protection, Neuherberg, Germany) family[9] and the ICRP (International Commission Radiological Protection, Ottawa, ON, Canada) voxelized reference male and female[10,11] were used in this study. The GSF/ICRP phantom models had all radiosensitive organs identified. The eight GSF voxel-based models were created from CT images with up to 131 organs and anatomic

structures segmented. The two ICRP reference male and female voxelized models were each based on modifications of two corresponding male and female GSF models of similar external dimensions. The GSF/ICRP voxelized models used in this study had the in-plane resolution subsampled from the original to decrease computation time.[9–11]

Additionally, to supplement the pediatric size range provided by the GSF/ICRP models, five voxelized patient models were created from anonymized head CT volume datasets of pediatric patients. These datasets were obtained from clinically indicated scans under IRB approval. Figure 1 contains an example of an axial slice of a 23-month-old pediatric head CT scan and the corresponding voxelized representation utilized in the MC simulations. All scans were acquired on a Siemens Sensation 64 multidetector row CT (MDCT) and were performed in the supine position. To create voxelized models of each patient's anatomy from the image data, voxels within each image series were modeled as either fat, water, muscle, bone, or air and were subdivided into one of 17 density levels depending on its CT number.[12] The density variations for the six different material designations are based on the CT scanner calibration curve and the linear relationship between mass density and electron density. This number of bins has been shown to be sufficient for CT dosimetry and has been validated in previous studies.[12,13] Individual organs were not segmented for these patient models, but brain parenchyma tissue was semiautomatically contoured and explicitly identified. The MCNPX model characteristics for all voxelized models used in this study are summarized in Table I. Detailed descriptions of scan length determination and patient size metrics in terms of D_w can be found in Sections 2.B and 2.C, respectively.

2.B. CT scanner and scanning protocol

The scanning protocol used in this investigation was taken from the AAPM Adult Routine Head CT protocol for a Siemens Sensation 64 MDCT.[14] Table II contains the CT scanning protocol used in this investigation. All simulations were performed as fixed tube current (FTC) helical scans with the voxelized models centered within the gantry and with the patient table removed. The scan range was defined from the top of the C1 lamina through the top of the calvarium.[14] The widest nominal collimation setting of 28.8 mm (measured beam width of 32.2 mm) on the Siemens scanner was used in the simulations because it is the most dose efficient collimation setting.[7] The AAPM's Routine Head CT protocol recommends either the gantry or head be tilted to reduce the dose to the lens of the eye;[14] however, for the scanner being modeled, helical scans are not performed with gantry tilt, so no tilt angle was used in these simulations.

2.C. Size metrics

D_w is a size metric referenced in AAPM Report 220 as the "x-ray attenuation of a patient in terms of a water cylinder having the same x-ray absorption" and was used in this study as a measure of patient size.[8] For the five pediatric patients, D_w was estimated at the center of the scan volume directly from the CT numbers (in Hounsfield units, HU) in their image data. For the GSF/ICRP models, it is not possible to directly calculate D_w since they are constructed with pixel data containing tissue identification numbers, not CT numbers. The D_w estimates for GSF/ICRP voxelized phantoms were instead obtained indirectly from a correlation between effective diameter and D_w.[7]

2.D. Monte Carlo simulations

All CT dose simulations for this investigation were conducted using a modified version of the radiation transport software package MCNPX (Monte Carlo N-Particle eXtended version 2.7.a).[13,15,16] Specifically, the source code was modified to model a MDCT scanner geometry and x-ray source trajectory. All simulations were conducted in photon transport mode with a 1 keV low-energy cutoff. This transport mode does not transport secondary electrons and instead assumes their energy to be deposited at the interaction site. All MC CT dosimetry for helical head scans were performed using an equivalent source model of the Siemens Sensation

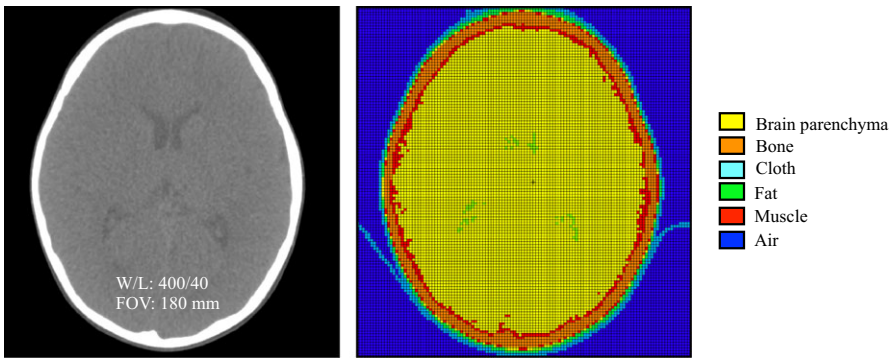

FIG. 1. (Left) Head CT image of a pediatric patient (Peds5) who underwent a routine CT head examination with window/level settings and reconstruction field of view (FOV). (Right) Monte Carlo representation of the patient produced using a CT number-based lookup table. The image on the right is color coded for the material designations for each voxel. [Color figure can be viewed at wileyonlinelibrary.com]

TABLE I. MCNPX model resolution characteristics, scan lengths, and D_w for GSF/ICRP phantom models and five patient models used in this investigation.

Name	Age	Gender	In-plane resolution	Image slices	Lateral width (mm)	Anterior–posterior width (mm)	Slice thickness (mm)	Scan length (cm)	D_w (cm)
Peds2[a]	7 days	Male	128 × 128	30	3.5	3.5	4.8	14.3	12.6
Peds1[a]	7 weeks	Male	128 × 128	24	3.5	3.5	4.8	11.6	10.6
Baby	8 weeks	Female	67 × 69	142	3.4	1.7	4.0	10.2	11.1
Peds3[a]	21 months	Female	128 × 128	36	3.9	3.9	4.8	16.7	15.6
Peds5[a]	23 months	Male	128 × 128	30	3.5	3.5	4.8	14.8	17.1
Peds4[a]	2 yr	Male	128 × 128	30	3.5	3.5	4.8	14.5	15.7
Child	7 yr	Female	64 × 64	144	6.2	6.2	8.0	14.8	17.2
Helga	28 yr	Female	64 × 64	114	7.8	7.8	10.0	14.5	18.2
Irene	32 yr	Female	66 × 66	348	7.5	3.8	5.0	15.8	17.1
Golem	38 yr	Male	64 × 64	220	8.3	8.3	8.0	15.6	18.3
Visible human	38 yr	Male	64 × 64	250	8.6	4.3	5.0	15.3	19.6
Regina	38 yr	Female	75 × 69	348	7.1	3.6	4.8	17.1	19.9
Donna	40 yr	Female	64 × 64	179	7.5	7.5	10.0	16.5	18.7
Rex	43 yr	Male	64 × 64	222	8.6	4.3	8.0	16.0	20.2
Frank	48 yr	Male	64 × 64	193	5.9	5.9	5.0	21.8	19.2

[a]Indicates a voxelized patient model created from image data obtained from clinically indicated scans.

TABLE II. Routine helical head FTC scanning protocol and associated $CTDI_{vol,16}$ per mAs for the scanner used in this investigation.

Parameter	Setting
kV	120
Rotation time (s)	0.5
Helical pitch	0.55
Nominal collimation (mm)	28.8
Bowtie filter	Standard
Central half value layer	8.9 mm Al
$CTDI_{vol,16}$/mAs (mGy/mAs)	0.24

64 MDCT scanner.[17] The equivalent source model, as previously described by Turner et al.[17], generates and incorporates scanner-specific x-ray spectra and bowtie filter profiles.

Concerning the voxelized models mentioned in Section 2.A, incorporation into MCNPX simulations required that each model be represented as a three-dimensional matrix of organ or nonanatomic material. Integer identification numbers were allocated for material descriptions based on elemental compositions of tissue substitutes and their densities as defined in ICRU Report 44.[10,12,18] Three-dimensional dose distributions of the entire head of each voxelized model were produced using the track-averaged rectangular mesh tally configuration (RMESH) in MCNPX. This tally configuration tracks particles through a mesh grid that is independent of the regular transport problem.[15] The mesh tally grid was defined to match the matrix size and resolution of each individual voxelized model to ensure that the dose on a per voxel basis was accurately estimated. The average energy deposition within each voxel was tallied in units of MeV/cm^3/source particle.[15] The resulting voxel-wise energy deposition maps were then divided by a density map to get units of MeV/g/source particle.

Normalization factors are necessary to convert dose per simulated source particle (mGy/source particle) to absolute dose per tube current time product (mGy/mAs). To achieve this, all MCNPX tally results were multiplied by a scanner, collimation, and beam energy-specific normalization factor.[19] Each simulation was performed with 10^8 photons to ensure a statistical uncertainty less than 2% for each individual mesh element. As mesh tallies were used to investigate dose distributions, the computation time was on the order of 10–15 h per voxelized model, depending on the resolution of the phantom. This study used computational and storage services associated with the Hoffman2 Shared Cluster provided by UCLA Institute for Digital Research and Education's Research Technology Group.

2.E. $CTDI_{vol}$ measurements

Since CT head scans performed in this study were all simulated scans, estimates of $CTDI_{vol}$ were needed for normalization purposes. Conventional $CTDI_{100}$ exposure measurements were taken at the center and peripheral position of a $CTDI_{vol,16}$ phantom with the scan parameters outlined in Section 2.B. Exposure measurements in milliroentgen (mR) were made with a standard 100-mm pencil ionization chamber (model: 10X6-3CT, Radcal, Monrovia, CA; calibrated by Radcal) coupled with a calibrated electrometer (MDH 1015, Radcal, Monrovia, CA; calibrated by Radcal) and converted to units of air kerma (mGy) using the conversion factor 1 mR = 0.00876 mGy. The 100-mm pencil ionization chamber and electrometer were calibrated for diagnostic energies with an energy dependence of ±5% for 3–20 mm AL HVL. The air kerma was then normalized by the tube current-rotation time product (mAs) used to take the initial measurements. $CTDI_{vol}$ was then calculated from the $CTDI_{100}$

measurements at the central and peripheral locations and was recorded on an air kerma per tube current-rotation time product basis (mGy/mAs).

2.F. Dose analyses

All dose values for each voxel in the patient models were obtained using mesh tallies as outlined in Section 2.D. Three regions were investigated in this study: (1) a small 0.6 cc volume at the center of the scan volume, (2) a 0.8–1.0 cm axial slab at the center of the scan volume, and (3) the entire scan volume. A representation of each tally region is shown in Fig. 2. Tally regions #1 and #2 were investigated as separate interpretations of "center of the volume." For tally region #1, a 0.6 cc volume was positioned at the center of the scan volume and the mean brain parenchyma dose values within all voxels in this small volume were averaged. Tally #1 was used to estimate the dose in a volume that is comparable to a Farmer chamber located in the center of the head. This configuration allows for a simplified comparison against empirical measurements wherein a Farmer chamber that is placed in the center hole of physical head CT dose phantoms (e.g., CIRS head CT phantoms[20]). The coefficient of variations (CV) was also recorded.

For tally region #2, dose values within a slab parallel to an axial plane at the center of the scan volume were identified. The thickness of the slab ranged from 0.8 to 1.0 cm, depending on the slice thickness of the voxelized phantom, as detailed in Table I in Section 2.A. Dose estimations within this slab consist of dose to the brain parenchyma and the bone surrounding it. Under this configuration, the mean of the dose voxels to both brain parenchyma and bone within the slab was calculated. The standard deviation and coefficient of variation for both brain parenchyma and bone dose within the slab were also calculated. Additionally, to consider the presence of both brain parenchyma and bone in tally #2 and tally #3, a mass-weighted average of dose contributions from both brain tissue and bone was calculated using Eq. (1),

$$D_{\text{wt-avg}} = \frac{D_{\text{bone}}M_{\text{bone}} + D_{\text{brain}}M_{\text{brain}}}{M_{\text{bone}} + M_{\text{brain}}} \quad (1)$$

where D_{bone} and D_{brain} are the mean dose contributions from bone and brain parenchyma, respectively, and M_{bone} and M_{brain} represent the mass contributions from bone and brain parenchyma, respectively. Similarly, the mean of the dose voxels of both brain parenchyma and bone within the entire scan volume was calculated as well as a mean mass-weighted average dose. The standard deviations and coefficients of variation for brain parenchyma and bone doses within the entire scan volume were also recorded. In this study, mean doses are designated using the nomenclature $D_{tissue,tally\ region}$ where *tissue* represents the tissue type and *tally region* represents one of the three tally regions. The tissue contents and doses calculated within each tally region are summarized in Table III.

All dose values were normalized by $\text{CTDI}_{\text{vol,16}}$. Consistent with AAPM Report 204, normalized dose values were parameterized as a function D_w using the following exponential relationship:

$$\frac{D_{tissue,tally\ region}}{CTDI_{vol}} = A \times e^{-B\times D_w} \quad (2)$$

where A and B (units of cm^{-1}) are regression constants for a given tissue classification. The coefficient of determination

TABLE III. Summary of tally regions, tissue contents within each tally region, and mean dose estimates measured.

Tally region	Tissue(s) in tally region	Doses calculated
#1: 0.6 cc volume	Brain parenchyma	$D_{brain,1}$
#2: central slab	Brain parenchyma, bone	$D_{brain,2}$, $D_{bone,2}$, $D_{wt\text{-}avg,2}$
#3: entire scan volume	Brain parenchyma, bone	$D_{brain,3}$, $D_{bone,3}$, $D_{wt\text{-}avg,3}$

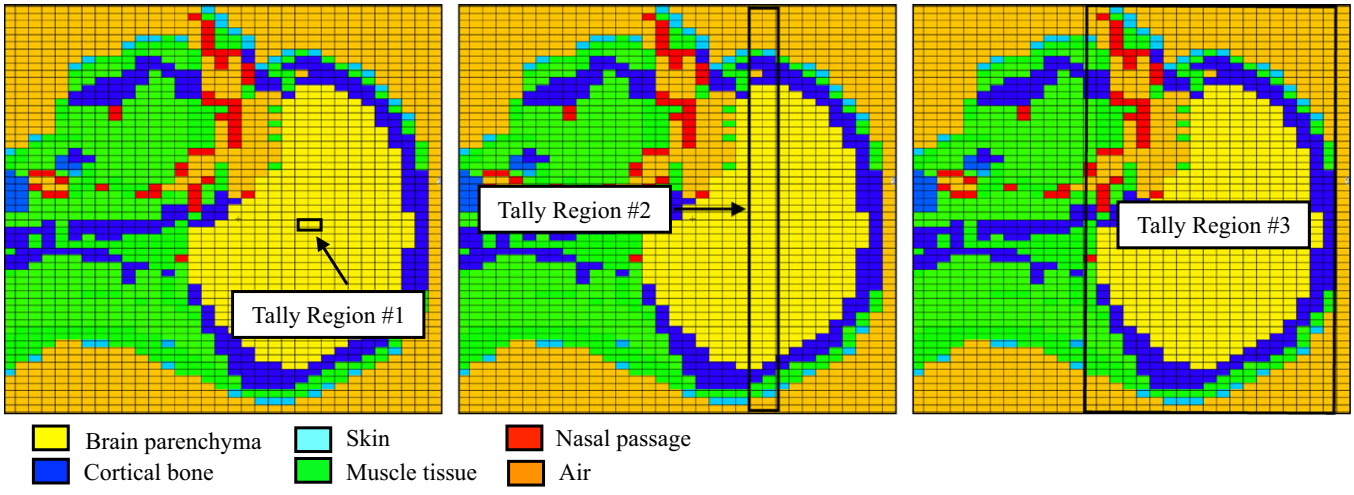

FIG. 2. MCNPX voxelized representation of ICRP male "Rex" depicting (1) the 0.6 cc volume positioned at the center of scan volume (tally region #1), (2) the 0.8–1.0 cm axial slab positioned at the center of the scan volume (tally region #2), and (3) the entire scan volume (tally region #3) as specified by the AAPM Routine Head CT[14] protocols with corresponding color-coded material designation for each voxel. [Color figure can be viewed at wileyonlinelibrary.com]

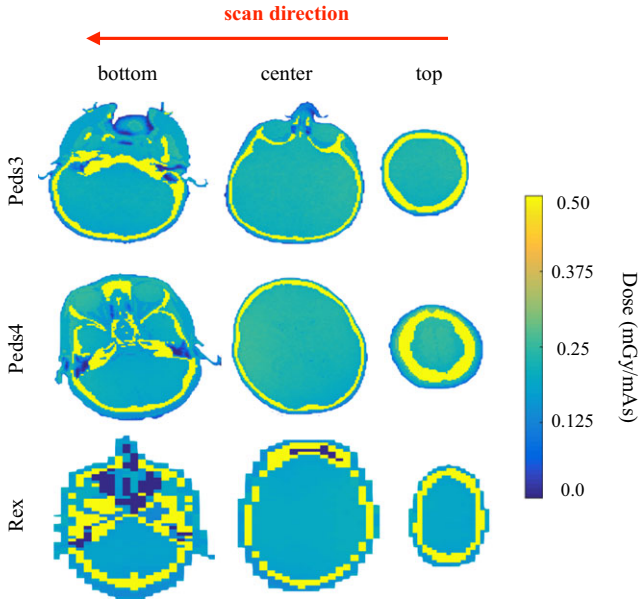

FIG. 3. Axial view of voxelized dose distribution maps for Peds3 (a), Peds4 (b), and Rex (c), respectively, at the top, center, and bottom of the scan volume. The red arrow at the top of the figure indicates the direction of the scan range. [Color figure can be viewed at wileyonlinelibrary.com]

(R^2) was used to assess the ability of the correlations to explain the proportion of variation explained by D_w.

Dose matrix analysis was performed using Matlab scripts (R2014b, TheMathWorks, Inc., Natick, MA, USA). Brain parenchyma dose voxels from all three tally regions were compared using the one-way analysis of variance (ANOVA). ANOVA was also performed to compare conversion factors from AAPM Report 204 for a $CTDI_{vol,16}$ phantom with normalized brain parenchyma dose voxels from the three tally regions. Bone doses for tally regions #2 and #3 were compared using a paired *t*-test. Additionally, differences between $D_{bone,2}$ and $D_{bone,3}$ were also tabulated and were defined as follows:

$$\frac{|\Delta D|}{(D_2 + D_3)/2} \times 100\% \quad (3)$$

where D_2 and D_3 are the doses corresponding to tally regions #2 and #3, respectively, and ΔD is the difference between D_2 and D_3. Similarly, the mass-weighted average doses for tally regions #2 and #3 were also compared using a paired *t*-test and the differences between $D_{wt\text{-}avg,2}$ and $D_{wt\text{-}avg,3}$ were calculated using Eq. (3) and were tabulated. ANOVA was also performed to compare conversion factors from AAPM Report 204 with mass-weighted average doses from tally regions #2 and #3. Statistical analyses were performed using GraphPad Prism 6.00 for Mac OS X (GraphPad Software, La Jolla, CA, USA, www.graphpad.com).

3. RESULTS

3.A. Mesh tally results

Dose distribution maps from the mesh tally simulations of three different voxelized models are shown in Fig. 3. These mesh tally results provide a graphical representation of the uniformity of the dose distribution within the brain parenchyma. Each of the following sections below describes the doses for each tissue group: brain parenchyma dose, bone dose, and the mass-weighted average of brain parenchyma and bone dose.

3.A.1. Brain parenchyma doses

$D_{brain,1}$, $D_{brain,2}$, and $D_{brain,3}$, for each voxelized model, can be seen in Table IV with values ranging from 0.188 to 0.292 mGy/mAs, 0.185 to 0.286 mGy/mAs, and 0.178 to 0.284 mGy/mAs, respectively. This table also shows that the CV was below 2.6%, 6.5%, and 9.4% within tally regions #1, #2, and #3, respectively, across all voxelized models and below 3.9% across all tally regions within each voxelized model. ANOVA analysis with multiple comparison showed that $D_{brain,1}$, $D_{brain,2}$, and $D_{brain,3}$ were not significantly different from each other [$F(2, 42) = 0.07$, $P = 0.93$].

3.A.2. Bone doses

$D_{bone,2}$ and $D_{bone,3}$, for each voxelized model, ranged from 0.664 to 1.040 mGy/mAs and 0.604 to 0.957 mGy/mAs, respectively, as indicated in Table V. The CV for $D_{bone,2}$ and $D_{bone,3}$ was less than 27% and 29%, respectively, within the individual patient models and differences of less than 12% were observed across all models. The differences between $D_{bone,2}$ and $D_{bone,3}$ were found to be statistically significant ($P < 0.0001$, using paired *t*-test).

3.A.3. Mass-weighted average

$D_{wt\text{-}avg,2}$ and $D_{wt\text{-}avg,3}$ ranged from 0.306 to 0.397 mGy/mAs and 0.380 to 0.472 mGy/mAs, respectively, across all

TABLE IV. Mean brain doses by tally region type with coefficients of variation within each tally region, and the coefficient of variation (CV) across tally regions for each patient.

	0.6 cc volume (#1)		Slab (#2)		Entire scan volume (#3)		
Name	$D_{brain,1}$ (mGy/mAs)	CV (%)	$D_{brain,2}$ (mGy/mAs)	CV (%)	$D_{brain,3}$ (mGy/mAs)	CV (%)	Across regions CV (%)
Peds2	0.257	2.6	0.254	4.2	0.273	5.0	3.9
Peds1	0.290	1.7	0.286	5.3	0.284	4.8	1.1
Baby	0.292	1.4	0.286	3.4	0.283	5.6	1.6
Peds3	0.230	2.5	0.226	4.0	0.238	7.3	2.6
Peds5	0.200	2.6	0.197	4.8	0.197	5.9	0.9
Peds4	0.217	2.0	0.215	4.8	0.216	6.7	0.5
Child	0.229	1.9	0.227	2.9	0.221	4.9	1.8
Helga	0.204	1.3	0.207	4.8	0.198	7.1	2.3
Irene	0.212	1.2	0.210	5.6	0.204	6.4	2.0
Golem	0.217	0.8	0.211	5.0	0.208	5.9	2.2
Visible human	0.188	1.7	0.187	6.5	0.180	9.4	2.4
Regina	0.216	2.5	0.215	5.3	0.207	7.8	2.3
Donna	0.210	2.8	0.214	4.4	0.203	7.1	2.7
Rex	0.197	0.8	0.195	3.9	0.189	5.9	2.1
Frank	0.190	1.4	0.185	5.0	0.178	9.2	3.3

voxelized models as indicated in Table VI. Differences of less than 27% were observed between $D_{wt\text{-}avg,2}$ and $D_{wt\text{-}avg,3}$ for each of the individual patient models. In addition, $D_{wt\text{-}avg,3}$ was consistently higher than $D_{wt\text{-}avg,2}$ across all patient models. These differences were statistically significant ($P < 0.0001$, using paired t-test).

3.B. Size-specific, scanner-independent dose estimates

3.B.1. Normalized brain parenchyma doses estimates and comparison with AAPM report 204 values

Figure 4 shows normalized brain parenchyma dose estimates for the three tally regions ($D_{brain,1}$, $D_{brain,2}$, and $D_{brain,3}$) parameterized as functions of D_w. For comparison, AAPM Report 204 conversion coefficients for the 16 cm pediatric body phantom as a function of D_w (Fig. 6 from that report) are included in the same figure. The R^2 values for normalized $D_{brain,1}$, $D_{brain,2}$, and $D_{brain,3}$ dose estimations were 0.86, 0.84, and 0.88, respectively. Results from the regression analysis are summarized in Table VII. ANOVA showed that there was no statistically significant difference between $D_{brain,1}$, $D_{brain,2}$, and $D_{brain,3}$ when compared to the AAPM Report 204 conversion factors based on $CTDI_{vol,16}$ [$F(3, 56) = 0.70$, $P = 0.56$]. However, it should be noted that estimates using AAPM report 204 conversion factors were consistently higher by 5–10% than those obtained using the regression equations for $D_{brain,1}$, $D_{brain,2}$, and $D_{brain,3}$ from Table VII.

3.B.2. Normalized bone doses estimates

Figure 5 contains normalized $D_{bone,2}$ and $D_{bone,3}$ parameterized as functions of D_w. The R^2 values for normalized $D_{bone,2}$ and $D_{bone,3}$ were 0.83 and 0.87, respectively. Results of the regression analysis are tabulated in Table VIII.

3.B.3. Normalized mass-weighted average doses and comparisons to AAPM report 204 values

Figure 6 shows normalized $D_{wt\text{-}avg,2}$ and $D_{wt\text{-}avg,3}$ parameterized as functions of D_w. The R^2 values for normalized $D_{wt\text{-}avg,2}$ and $D_{wt\text{-}avg,3}$ were 0.39 and 0.51, respectively. ANOVA revealed a statistically significant difference between AAPM Report 204 conversion factors and normalized $D_{wt\text{-}avg,2}$ and

TABLE V. Mean bone doses by tally region type with coefficients of variation within each tally region and differences between the means of each region.

	Slab (#2)		Entire scan volume (#3)		
Name	$D_{bone,2}$ (mGy/mAs)	CV (%)	$D_{bone,3}$ (mGy/mAs)	CV (%)	Difference (%)
Peds2	0.929	7.5	0.916	11	1.4
Peds1	0.917	27	0.894	29	2.5
Baby	1.040	6.1	0.957	14	8.3
Peds3	0.839	16	0.768	21	8.8
Peds5	0.857	14	0.768	19	11
Peds4	0.759	18	0.731	24	3.8
Child	0.792	5.0	0.733	15	7.8
Helga	0.734	10	0.651	16	12
Irene	0.730	9.0	0.697	12	4.7
Golem	0.723	8.1	0.688	15	11
Visible human	0.673	13	0.603	18	5.3
Regina	0.730	9.4	0.693	11	5.0
Donna	0.750	8.8	0.680	13	9.7
Rex	0.661	8.3	0.636	11	3.9
Frank	0.664	10	0.604	17	9.4

TABLE VI. The mass-weighted average of brain and bone dose for tally regions #2 and #3 ($D_{wt\text{-}avg,2}$ and $D_{wt\text{-}avg,3}$) and the differences between the means of each region.

Name	Slab (#2) $D_{wt\text{-}avg,2}$ (mGy/mAs)	Entire scan volume (#3) $D_{wt\text{-}avg,3}$ (mGy/mAs)	Difference (%)
Peds2	0.338	0.412	20
Peds1	0.366	0.436	18
Baby	0.397	0.472	17
Peds3	0.359	0.399	11
Peds5	0.326	0.408	22
Peds4	0.326	0.395	19
Child	0.324	0.397	20
Helga	0.311	0.398	25
Irene	0.328	0.417	24
Golem	0.351	0.411	16
Visible human	0.332	0.380	13
Regina	0.306	0.402	27
Donna	0.350	0.427	20
Rex	0.317	0.379	18
Frank	0.361	0.401	11

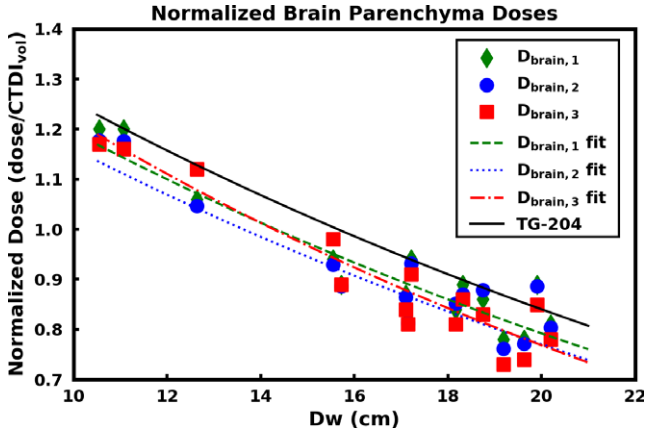

FIG. 4. Brain parenchyma dose estimations for the three tally regions ($D_{brain,1}$, $D_{brain,2}$, and $D_{brain,3}$) normalized by $CTDI_{vol,16}$ are plotted as a function of D_w along with the associated regression fits. AAPM Report 204 conversion factors based on $CTDI_{vol,16}$ are also plotted for comparison. [Color figure can be viewed at wileyonlinelibrary.com]

TABLE VII. Regression analysis results for $D_{brain,1}$, $D_{brain,2}$, and $D_{brain,3}$, along with AAPM report 204 regression curve coefficients.

Normalized dose	A	B (cm^{-1})	R^2
$D_{brain,1}$	1.80	0.041	0.86
$D_{brain,2}$	1.74	0.041	0.84
$D_{brain,3}$	1.93	0.046	0.88
AAPM report 204	1.87	0.039	–

$D_{wt\text{-}avg,3}$ dose estimations [$F(2,42) = 168.1$, $P < 0.0001$]. Results from the regression analysis are summarized in Table IX. It should be noted here that the AAPM Report 204 values are consistently lower than the $D_{wt\text{-}avg,2}$ and $D_{wt\text{-}avg,3}$

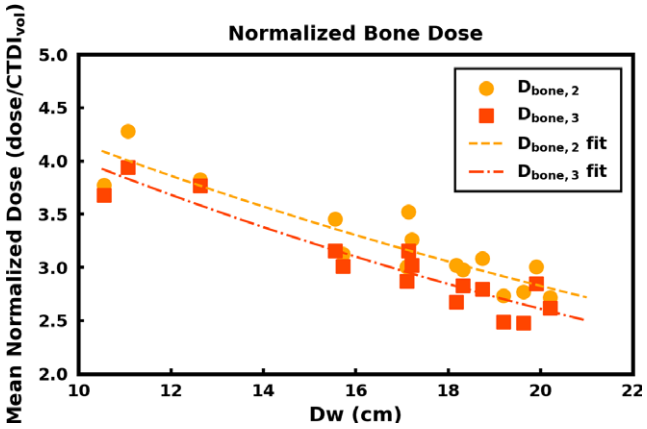

FIG. 5. Normalized $D_{bone,2}$ and $D_{bone,3}$ with associated regression fits. [Color figure can be viewed at wileyonlinelibrary.com]

TABLE VIII. Regression analysis for normalized $D_{bone,2}$ and $D_{bone,3}$.

Normalized dose	A	B (cm^{-1})	R^2
$D_{bone,2}$	6.17	0.039	0.83
$D_{bone,3}$	6.17	0.043	0.88

dose estimations as indicated in Fig. 6. The fit coefficients for AAPM Report 204 are the same as those in Table VII.

4. DISCUSSION AND CONCLUSIONS

In this study, MC simulation methods were performed to obtain estimates of brain parenchyma and bone dose from patients of different sizes with different tally configurations that could be used as a basis for determining SSDE conversion coefficients for routine, helical head CT examinations. Two different tally configurations were considered as possible candidates for the condition that the measured dose be in the "center scan volume" as described in AAPM Report 204.[5] In addition, a third tally configuration estimated the dose to the entire scan volume of each patient for comparison. A mass-weighted average dose quantity was used to consider the presence of bone in the central slab tally configuration, as well for the entirety of the scan volume. Lastly, normalized brain parenchyma dose estimations under all the three tally configurations and normalized mass-weighted average dose quantity for the both slab and the entire scan volume were compared with conversion coefficients from AAPM Report 204 based on $CTDI_{vol,16}$.

Normalized $D_{brain,1}$, $D_{brain,2}$, and $D_{brain,3}$ had R^2 values of 0.86, 0.84, and 0.88, respectively. This indicates that D_w provides good correlative function for the normalized brain parenchyma dose using the three tally configurations investigated in this study. Unlike the study conducted by McMillan et al., which only investigated normalized organ doses,[7] the current study employed meshed tallies to map dose distributions on a per voxel basis. Using this approach, $D_{brain,1}$, $D_{brain,2}$, and $D_{brain,3}$ were found to be homogeneous

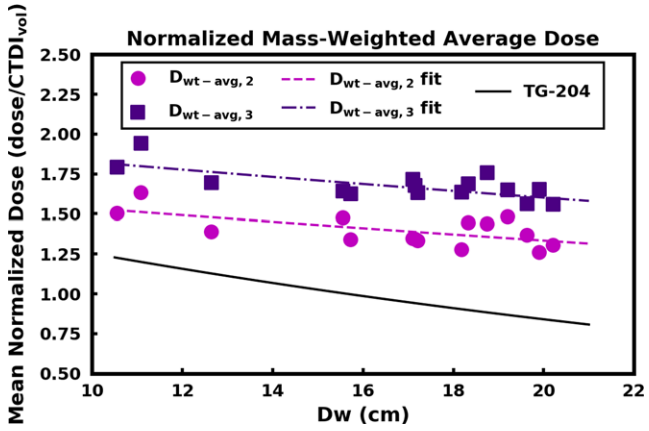

FIG. 6. Normalized mass-weighted average dose to the brain parenchyma and cortical bone for tally regions #2 and #3 ($D_{wt\text{-}avg,2}$ and $D_{wt\text{-}avg,3}$) along with the associated regression fits. AAPM Report 204 conversion factors based on $CTDI_{vol,16}$ are also plotted for comparison. [Color figure can be viewed at wileyonlinelibrary.com]

TABLE IX. Regression analysis for normalized $D_{wt\text{-}avg,2}$ and $D_{wt\text{-}avg,3}$.

Normalized dose	A	B (cm^{-1})	R^2
$D_{wt\text{-}avg,2}$	1.76	0.014	0.39
$D_{wt\text{-}avg,3}$	2.08	0.013	0.51

with CVs below 10% across all voxelized models and below 4% across all tally regions within each voxelized model. The implications of these results are twofold. The first is that if "center of the scan volume" is defined as a small, central volume ($D_{brain,1}$) or a central slab within the brain parenchyma ($D_{brain,2}$), then normalized doses within these regions should yield similar results for a head SSDE. The second is that since the dose to the brain is fairly uniform, a dose measure from either of these two tally regions would be similar to dose to the entire brain ($D_{brain,3}$).

$D_{bone,2}$ and $D_{bone,3}$ dose estimations had CVs as high as 29% and 27%, respectively. Variations in surface dose as high as 30% for helical scans were previously observed by Zhang et al.[21] as a consequence of wider beam collimations and tube start angle. When investigating the surface dose profile of a $CTDI_{vol,32}$ phantom using MC, for example, Zhang et al. reported substantial dose peaks when utilizing a pitch of less than one and when the simulated beam width was wider than the nominal beam width.[21] A similar effect was seen when investigating the variability in surface dose in anthropomorphic phantoms in the abdominal and thoracic regions, whereby a pitch of 0.75 was shown to result in a 37% increase in surface dose.[21] The results of this study indicate that the dose variations observed within voxels of the bone could be due to surface dose variations, particularly given the use of the low pitch and wide beam collimations recommended in the AAPM's Adult Routine Head CT Protocol.[14]

The R^2 values for normalized $D_{bone,2}$ and $D_{bone,3}$ were 0.83 and 0.87, respectively, indicating that D_w is a satisfactory size metric for parameterization of normalized bone dose either for a central slab (i.e., tally region #2) or for entirety of the head (i.e., tally region #3). The motivation for investigating dose to bone as a function of patient size comes from the fact that, within the cranium of pediatric patients, there is a fair amount of red bone marrow (RBM). The amount of RBM in the head (relative to the entire body) is 12% for children 10 yr of age and up to 29% for infants.[22,23] The cranium is composed of the inner and outer layers of cortical bone that enclose bone spongiosa, wherein RBM, yellow bone marrow (YBM), and trabecular bone are found.[23] RBM is the primary tissue of interest for the radiogenic risk of leukemia and is considered highly radiosensitive, as reflected by the high tissue weighting designation in ICRP 103 (w_T = 0.12).[24] In this study, RBM and YBM were not modeled. The cranial microdosimetry necessary to accurately assess RBM dose is beyond the scope of this study, as is assessing the leukemia risk associated with head CT procedures. RBM and YBM doses could, in principle, be calculated using fluence-to-dose response functions or dose enhancement factors (e.g., the Annex on Skeletal Dosimetry in ICRP Publication 116[25]). This would, however, require age- and bone-specific dose response functions or enhancement factors, which were not available for this current study. SSDE was only intended to estimate patient dose using metrics of radiation output displayed by scanners and was not intended to assess cancer risk from CT procedures.[5] In routine head CT examinations, although the cortical bone would provide some shielding for the spongiosa containing RBM, RBM within the cranium would still receive some appreciable amount of radiation dose. The potential effects of RBM dose should be taken into consideration as a consequence of the scanning techniques used in routine head CT examinations, particularly for pediatric patients.[24,26]

In accordance with the second interpretation of "center of scan volume," this study also investigated dose to a central slab of the head, which consists of both bone and brain parenchyma. A mass-weighted average of the dose contributions from both bone and brain parenchyma was devised to take into consideration the presence of both tissue types. The R^2 values for normalized $D_{wt\text{-}avg,2}$ and $D_{wt\text{-}avg,3}$ were 0.39 and 0.51, respectively. The loss of an exponential relationship effects with respect to the normalized mass-weighted average dose as a function of patient size can be explained by considering the relationship between bone mass (and tissue mass) fraction of the head as a function of patient size. The mass of bone increases with age which competes with the decreasing exponential of normalized dose vs patient size. Weighting normalized doses of brain parenchyma and bone by their respective masses accounts for the effects of size of the patients in effect, making the relationship of normalized weighted average dose more linear with respect to patient size. Additionally, the statistically significant difference observed between normalized $D_{wt\text{-}avg,2}$ and $D_{wt\text{-}avg,3}$ and AAPM Report 204 can be attributed to the fact that, as mentioned in Section 3.B.3, the conversion coefficients in AAPM Report 204 were devised for the abdomen region, which contains a small amount of bone relative to the

percentage of soft tissue. The values reported in AAPM Report 204 were consistently lower than normalized $D_{wt\text{-}avg,2}$ and $D_{wt\text{-}avg,3}$ due to taking the dose contributions of bone into consideration.

In several places in this study dose estimates were compared with AAPM Report 204 coefficients of SSDE to assess the generalizability of those coefficients to helical head scans when estimating dose to the center of the scan volume. When estimating brain dose, Fig. 4 and Table VII showed the $D_{brain,1}$, $D_{brain,2}$, and $D_{brain,3}$ estimates and the regression fits for each of these estimates as well as the SSDE-based estimates and coefficients. A one-way ANOVA showed no statistically significant difference between the estimates obtained from the regression fits and those obtained using AAPM Report 204 conversion factors; however, the conversion factors from AAPM Report 204 were consistently higher than those provided by the regression fits of $D_{brain,1}$, $D_{brain,2}$, and $D_{brain,3}$. The differences observed between AAPM Report 204 and normalized $D_{brain,1}$, $D_{brain,2}$, and $D_{brain,3}$ can be attributed to the fact that the AAPM Report 204 conversion factors were originally devised to estimate dose to the center of the scan volume for the abdomen, which is a homogenous region comprised of soft tissue. The head, in contrast, is comprised of the soft-tissue brain parenchyma encased in a layer of bone. The presence of the bone provides an inherent source of shielding for the brain parenchyma, which decreases the normalized dose of the brain parenchyma relative to the normalized dose to the center of the scan volume for the abdomen.

When estimating the mass-weighted average dose to brain parenchyma and cortical bone, Fig. 6 and Table IX showed the $D_{wt\text{-}avg,2}$ and $D_{wt\text{-}avg,3}$ estimates and the regression fits for each of these estimates, as well as the conversion factors from AAPM Report 204. This time, the one-way ANOVA analysis did show a statistically significant difference between the estimates obtained from the regression fits and those obtained using AAPM Report 204 conversion factors. In addition, the conversion factors from AAPM Report 204 were shown to be consistently lower by 32–50% than those provided by the regression fits of $D_{wt\text{-}avg,2}$ and $D_{wt\text{-}avg,3}$. Thus, the conversion factors found in AAPM Report 204 do not appear to be applicable when the dose to bone is included.

There are some limitations to this study. This study only investigated dose distributions from voxelized phantom models and voxelized patient data from a single scanner model. In order to devise an official SSDE for head CT examinations, the data presented in this study may be combined with other physical air kerma measurements of head-sized phantoms and MC simulations from different scanner models as was done for AAPM Report 204.[5] Moreover, the voxelized phantom models used in this investigation were of low spatial resolution. Despite the low resolution of the phantoms, dose distribution within the brain parenchyma was still observed to be fairly uniform. This dose uniformity was observed even for the voxelized patient models, which have much higher resolution. However, the low resolution could affect the accuracy of surface bone dose (and mass-weighted average dose) due to volume averaging used to make coarser voxels. Additionally, the patient table was not considered in these simulation, the omission of which could lead to an overestimation of patient dose.[27] However, this overestimation is expected to be under 10% relative to doses considering the inclusion of the table.[27]

In summary, this study developed conversion coefficients for routine helical head CT procedures using MC methods and voxelized patient models for two interpretations of "center of the scan volume" that may be used in a manner similar to those described in AAPM Report 204.[5] In addition, normalized dose coefficients were estimated as a function of patient size for both bone and a mass-weighted average of brain and bone, all in the middle of the scan volume. These may contribute to the efforts to report size-specific doses arising from CT examinations of the head.

ACKNOWLEDGMENTS

This work was supported in part by a grant from the NIBIB (R01-EB017095) and by a grant from the NIH (T32-EB002101). J.M.B is supported in part by NIH grants (R01-CA181081, R01-EB025829, and R01-CA214515). A.M.H is supported in part by NIH grant R01-CA18108. C.H.M. receives research support from Siemens Healthcare. M.M.G's department has a master research agreement with Siemens Healthcare.

[a]Author to whom correspondence should be addressed. Electronic mail: ahardy@mednet.ucla.edu; Telephone: (310) 481-7558.

REFERENCES

1. Smith-bindman R, Moghadassi M, Wilson N, et al. Radiation doses in consecutive CT examinations from five University of California Medical Centers. *Radiology*. 2015;277:134–141.
2. McCollough CH. CT dose: how to measure, how to reduce. *Health Phys*. 2008;95:508–517.
3. McNitt-Gray MF. AAPM/RSNA physics tutorial for residents: topics in CT radiation dose in CT1. *Radiographics*. 2002;22:1541–1553.
4. Turner AC, Zhang D, Khatonabadi M, et al. The feasibility of patient size-corrected, scanner-independent organ dose estimates for abdominal CT exams. *Med Phys*. 2011;38:820–829.
5. AAPM Task Group 204. *Size-Specific Dose Estimates (SSDE) in Pediatric and Adult Body CT Examinations*. College Park, MD: American Association of Physicists in Medicine; 2011.
6. Moore BM, Brady SL, Mirro AE, Kaufman RA. Size-specific dose estimate (SSDE) provides a simple method to calculate organ dose for pediatric CT examinations. *Med Phys*. 2014;41:1–10.
7. McMillan K, Bostani M, Cagnon C, Zankl M, Sepahdari AR, McNitt-Gray M. Size-specific, scanner-independent organ dose estimates in contiguous axial and helical head CT examinations. *Med Phys*. 2014;41:121909.
8. AAPM Task Group 220. *Use of Water Equivalent Diameter for Calculating Patient Size and Size-Specific Dose Estimates (SSDE) in CT*. College Park, MD: American Association of Physicists in Medicine; 2014.
9. Petoussi-Henss N, Zankl M, Fill U, Regulla D, Zanki M. The GSF family of voxel phantoms. *Phys Med Biol*. 2002;47:89–106.
10. International Commission on Radiological Protection. Adult reference computational phantoms. ICRP Publ 110 Ann ICRP 39; 2009:(2).
11. Zankl M, Eckerman KF, Bolch WE. Voxel-based models representing the male and female ICRP reference adult – the skeleton. *Radiat Prot Dosimetry*. 2007;127:174–186.

12. Demarco JJ, Solberg TD, Smathers JB. A CT-based Monte Carlo simulation tool for dosimetry planning and analysis. *Med Phys*. 1998;25:1–11.
13. Bostani M, Mueller JW, McMillan K, et al. Accuracy of Monte Carlo simulations compared to in-vivo MDCT dosimetry. *Med Phys*. 2015;42:1080.
14. American Association of Physicists in Medicine. Adult Routine Head CT Protocols Version 2.0 [Internet]; 2016:1–20. Available from: https://www.aapm.org/pubs/CTProtocols/documents/AdultRoutineHeadCT.pdf
15. Pelowitz DB. *MCNPX User's Manual*. Version 2.7.0, Los Alamos National Laboratory, LA-CP-11-00438. Los Alamos, New Mexico: LANL; 2011.
16. AAPM Task Group 195. *Monte Carlo Reference Data Sets for Imaging Research*. College Park, MD: American Association of Physicists in Medicine; 2015.
17. Turner AC, Zhang D, Kim HJ, et al. A method to generate equivalent energy spectra and filtration models based on measurement for multidetector CT Monte Carlo dosimetry simulations. *Med Phys*. 2009;36:2154–2164.
18. The International Commission on Radiation Units and Measurements. Tissue substitutes in radiation dosimetry and measurement. ICRU Report No. 44, ICRU, Bethesda, MD; 1989.
19. DeMarco JJ, Cagnon CH, Cody DD, et al. A Monte Carlo based method to estimate radiation dose from multidetector CT (MDCT): cylindrical and anthropomorphic phantoms. *Phys Med Biol*. 2005;50:3989–4004.
20. Computerized Imaging Reference Systems Inc. Tissue Equivalent CT Dose Phantoms [Internet]; 2013 [cited 2018 Sep 20]. Available from: http://www.cirsinc.com/file/Products/007TE/007TE DS 063017(1).pdf
21. Zhang D, Savandi AS, Demarco JJ, et al. Variability of surface and center position radiation dose in MDCT: Monte Carlo simulations using CTDI and anthropomorphic phantoms. *Med Phys*. 2009;36:1025–1038.
22. ICRP 70. Basic anatomical & physiological data for use in radiological protection - the skeleton. *Ann ICRP*. 1995;25:1–80.
23. Cristy M. Active bone marrow distribution as a function of age in humans. *Phys Med Biol*. 1981;26:389–400.
24. ICRP. The 2007 Recommendations of the International Commission on Radiological Protection. ICRP Publ 103 Ann ICRP 37; 2007.
25. Petoussi-Henss N, Bolch WE, Eckerman KF, et al. Conversion coefficients for radiological protection quantities for external radiation exposures. *Ann ICRP* [Internet] 2010;40:1–257.
26. Pearce MS, Salotti JA, Little MP, et al. Radiation exposure from CT scans in childhood and subsequent risk of leukaemia and brain tumours: a retrospective cohort study. *Lancet*. 2012;380:499–505.
27. Nowik P, Bujila R, Kull L, Andersson J, Poludniowski G. The dosimetric impact of including the patient table in CT dose estimates. *Phys Med Biol* [Internet]. 2017;62:N538–N547.